The increasing surface and tropospheric ozone level in Antarctica and their possible drivers

P. Kumar[1], J. Kuttippurath[1,*], Peter von der Gathen[2], I. Petropavlovskikh[3], B. Johnson[4], A. McClure-Begley[3], P. Cristofanelli[5], P. Bonasoni[5], M. E. Barlasina[6], and R. Sánchez[6]

[1] CORAL, Indian Institute of Technology Kharagpur, 721302 Kaharagpur, India

[2] Alfred Wegener Institute for Polar and Marine Research, Postdam, Germany

[3] Cooperative Institute for Research in Environmental Sciences, University of Colorado, Boulder, USA

[4] NOAA, ESRL Global Monitoring Laboratory, Boulder, CO, USA

[5] CNR Institute of Atmospheric Sciences and Climate, 40129 Bologna, Italy

[6] Servicio Meteorológico Nacional, Vigilancia de la Atmosfera y Geofísica, Buenos Aires, Argentina

*Corresponding author: Dr. Jayanarayanan Kuttippurath,
CORAL, IIT Kharagpur,
Kharagpur-721302, India.
E-mail: jayan@coral.iitkgp.ac.in

Short Title: Tropospheric ozone in Antarctica

Keywords: Antarctica, Tropospheric ozone, Tropopause, MLR, DLM, Trajectory, Clustering

ABSTRACT

A comprehensive analysis of the temporal evolution of tropospheric ozone in Antarctica using more than 25 years of surface and ozonesonde measurements reveals significant changes in tropospheric ozone there. It shows a positive trend in ozone at the surface, lower and mid-troposphere, but a negative trend in the upper troposphere. We also find significant links between different climate modes and tropospheric ozone in Antarctica; and observe that changes in residual overturning circulation, the strength of the polar vortex, and stratosphere-troposphere exchange make noticeable variability in tropospheric ozone. Therefore, this study alerts of increasing ozone concentration in Antarctica, which would have a profound impact on the future climate of the region as tropospheric ozone has warming feedback to the Earth's climate.

INTRODUCTION

Ozone is vital for existence of life on Earth as it absorbs the ultra-violet (UV, 200–315 nm) radiations in the stratosphere (90% of total atmospheric ozone)[1]. On the other hand, tropospheric ozone is a major air pollutant causing severe effects on human health[2], agricultural production[3] and is an important greenhouse gas with a global warming potential 1000 times that of CO_2, although it is only 10% of total column ozone[4,5]. Tropospheric ozone is formed by oxidation of its precursors of both anthropogenic (industry and transportation) and natural (lightning, biomass burning and biogenic emissions) origin such as methane (CH_4), carbon monoxide (CO), volatile organic compounds (VOCs) and nitrogen oxides (NO_x)[6]. It is also transported from stratosphere to troposphere across the tropopause (about 10% of tropospheric production) due to synoptic wave breaking in the stratosphere[7].

As ozone has a residence time of a month in the free troposphere, the inter-hemispherical transport can contribute significantly to the ozone budget in each hemisphere, even in remote locations[8]. Changes in air-mass transport associated with large-scale dynamical modes such as the Southern Annular Mode (SAM)/Antarctic oscillation (AAO) and El Niño and southern oscillation (ENSO) contribute to large inter-annual and decadal variability[8] and influence the strength of polar vortex and stratosphere-troposphere exchange (STE)[9,10]. A number of studies have shown that the ozone loss in stratosphere is enhanced by increase in greenhouse gases[11], changes in atmospheric circulation (positive trend in AAO manifested as strengthening of polar vortex and poleward shift of jet) and lower stratospheric cooling (up to 10°C in October and November). The cooling can shift the tropopause altitude and transport ozone to the troposphere with a lag of about a month, and can significantly affect the surface climate there[12]. Although the inter-annual variability can trigger significant change in tropospheric ozone, it is still challenging to attribute the origin of tropospheric ozone variability due to complex interactions between chemistry and dynamics there.

A number of studies have reported the increasing tropospheric ozone in both hemispheres due to anthropogenic emissions and climate variability.[13–29] For example, Wespes et al. [9] analysed tropospheric ozone trends with 8 years (2008–2016) of ozone profiles from Infrared Atmospheric Sounding Interferometer (IASI) using solar flux, Quasi-biennial oscillation (QBO), AAO and ENSO as geophysical drivers. They found that ENSO perturbed ozone variability from the tropics to the polar latitudes in both hemisphere. Zeng et al. [14] analysed ozone trends and variability from 28 years (1987–2014) of ozonesonde records at Lauder (a mid-latitude station) and found a statistically significant positive trend in the lower troposphere and a negative trend in the upper troposphere and lower stratosphere (UTLS) region. The trends in the lower troposphere are

consistent with increasing temperature and decreasing humidity at the surface whereas those in UTLS are primarily driven by an upward trend of the tropopause height. They found that both methane and non-methane ozone precursors cause ozone increases in the troposphere. Also, Five out of seven southern hemispheric stations (including South Pole and Neumayer) showed positive trends in surface ozone as analysed by Cooper et al. [16] using monthly surface ozone anomalies.

Similarly, Lu et al. [27] reported increase in tropospheric ozone in southern hemisphere (SH) over 1990–2015 by using in-situ and satellite observations. In contrast to the results of Zeng et al. [14], they found that increasing anthropogenic emissions were not the prominent drivers of ozone increase there. Instead, the positive trend was driven by changes in meteorology (poleward expanding Hadley circulation in particular). Legrand et al. [21] analysed long-term variability of surface ozone during summer at Dumont d'Urville (DDU) and Concordia, and compared it to that at South Pole (inland site), Syowa, Neumayer and Halley (coastal sites). Measurements at both stations showed negative trends due to changes in synoptic transport and reduction in NO_x production from the snowpack. However, DDU showed an increasing in ozone during winter, which may be due to the influence of STE. Masclin et al. [17] found the linkage of elevated ozone at the West Antarctic Ice Sheet (WAIS) divide in West Antarctica to air mass transport from the high altitude plateau region. Hsu et al. [22] analysed the role of STE in variation of tropospheric ozone in both hemispheres. They found that STE explains a large fraction of changes in tropospheric ozone (7–8 DU) equivalent to the late summer photochemical production. The QBO explained about 45% of STE variability whereas the contributions from ENSO and AAO were negligible. They predicted 10% reduction in STE attributed to stratospheric ozone depletion during 1979–2004.

However, there is still a dearth of comprehensive studies on temporal evolution of tropospheric ozone in Antarctica. Therefore, we explore the long-term trend, variability and its drivers, and transport of tropospheric ozone to the southern polar region. We analyze all available measurements from the ground-based Antarctic stations and ozonesonde observations since 1985 to determine the long-term tropospheric ozone trends, using Simple Linear Regression (SLR), Multiple Linear Regression (MLR) and Bayesian Dynamic Linear Model (DLM) with the help of dynamical and chemical factors that affect ozone variability. In addition, we also use meteorological data from National Centers for Environmental Prediction (NCEP) to feed the Hybrid Single Particle Lagrangian Integrated Trajectory (HYSPLIT) model of National Oceanic and Atmospheric Administration (NOAA) in order to investigate STE and identify the sources of ozone at various tropospheric altitudes. A better understanding of the variations in air mass

transport is an essential prerequisite for identifying the different factors affecting the tropospheric ozone variability in Antarctica.

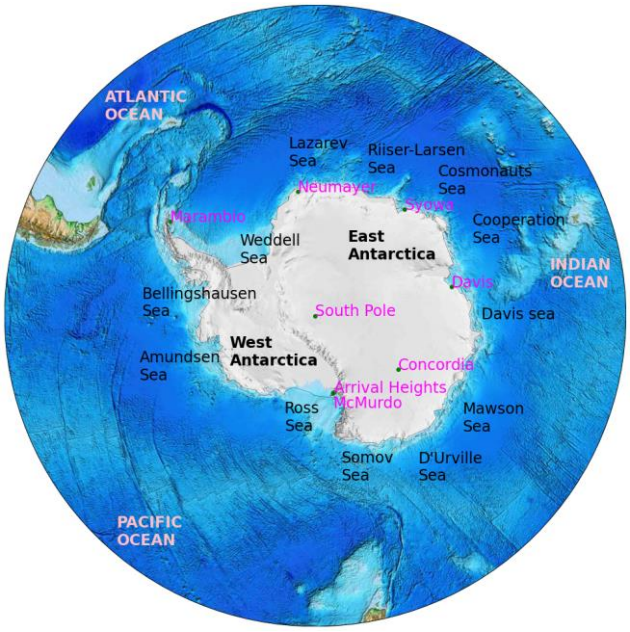

Figure 1: Locations of ozone measuring stations in Antarctica considered in this study.

MATERIAL AND METHODS

Surface observations and Ozonesonde measurements

We use the ground based surface ozone measurements from Arrival Heights, Concordia, Neumayer, South Pole and Syowa and ozonesonde measurements from Davis, Marambio, McMurdo, Neumayer, South Pole and Syowa. The coordinates of surface and sonde measurements are shown in Fig. 1 and are also given in Table S1. The frequency of ozonesonde measurements from individual station is very small in a month. The ozonesondes provide high vertical resolution profiles of ozone, temperature, pressure and humidity and include both electrochemical cell and carbon-iodide type of measurements[30]. The ozonesonde measurements have an accuracy of 5-10%. We estimate the tropopause height with ozonesonde temperature data using World Meteorology Organization (WMO) definition of lapse rate tropopause, also called thermodynamic tropopause, which is defined as the lowest altitude where the lapse rate is less than 2 K/km and the average lapse rate from this height up to 2 km above is also below 2 K/km[31].

As there are two types of stations involved in this study (coastal and plateau), we expect their ozone characteristics to be different from each other. Therefore, we calculate the weighted mean of all available measurements in a month and its reduced chi-square corrected standard error for long-term analysis of ozone trend for the Antarctic region[32, 33] wherein weight accounts for the differences in instrument types employed at various stations and their geographical locations (coastal and inland). Further details about the calculation and discussion of the weighted mean and standard error can be found in supplementary material.

Since we have only one station (Syowa) measurements before 1992, we did not consider these measurements for long-term analysis and trend calculation. In addition, surface ozone has measurement gaps. For example, Arrival Heights surface ozone measurements have gaps during October–December 2016 and December 2017, South Pole shows gaps during September–December 2016 and August–December 2017, and Concordia measurements have gaps during August–September 2006, September–December 2007 and January–February 2013. We have imputed the missing data in surface ozone observations using its monthly climatological mean for the trend estimation.

Clustering of ozone profiles

Clustering of ozone profiles into groups with similar profile shape is a good way of studying ozone variability without considering the month or season of profiles. We use self-organizing map (SOM) based cluster analysis to categorize ozone profiles. SOM is an artificial neural network (ANN), which uses competitive, unsupervised learning to produce low-dimensional representation of high-dimensional data preserving topological relations among them in the process. In SOM, each ozone profile is assigned to a predefined number of nodes according to profile shape similarity, which is determined by minimizing the Euclidean distance between nodes and corresponding ozone profiles. Initial nodes are found by linear interpolation between two principal components of ozone profiles ensuring the coverage of large variability in the dataset. Final clusters represent profiles that could be influenced by dynamics and chemistry. Please see Stauffer et al. [34] for detailed discussions about SOM. Here we use 2×2 SOM nodes with 4 clusters to get robust statistics, avoiding too few or too many clusters (See supplementary material for discussion about 3×3 and 4×4 SOM nodes).

Trajectory generation and clustering

We calculate 15 days backward trajectories on daily basis for all seasons using PySPLIT[35], a python toolkit for HYSPLIT model from National Oceanic and Atmospheric Administration (NOAA)[36].

The meteorological data are considered from National Centers for Environmental Prediction (NCEP) with 2.5° latitude-longitude grids. The trajectory analyses were performed to find the air mass transport to the stations at different altitudes from the ground level (500, 1000, 5000, 8000 and 9000 m). Here, 500 and 1000 m [agl] represent the lower troposphere, 5000 m represents the middle troposphere and 8000 and 9000m represent the UTLS (upper troposphere and lower stratosphere).

We cluster trajectories with K-Means clustering using non-parametric features extracted from discrete wavelet transform (DWT) based decomposition of projected backward trajectories that encode the time-varying information of the trajectories. Here, we compute the DWT coefficients using the single-level implementation of Mallat's algorithm with Haar wavelets to capture the variations in trajectories[37]. We build a feature vector comprising of approximation DWT coefficients (C^{xi}, C^{yi}) of a trajectory i as follows:

$$f_i = (f^{x_i}, f^{y_i})$$

where

$$f^{x_i} = \left(C_{min}^{x_i}, C_{25}^{x_i}, C_{50}^{x_i}, C_{75}^{x_i}, C_{max}^{x_i}\right) \quad (1)$$

Here, C_n represents the n^{th} percentile of the distribution of DWT coefficients C.

f_i provides comprehensive description of trajectory i as it captures the overall distribution of coefficients non-parametrically using a set of coefficient statistics that includes the minimum coefficient (C_{min}), 25th percentile (C_{25}), median (C_{50}), 75th percentile (C_{75}) and the maximum value (C_{max}). This approach does not require the trajectories to have equal length. The clustering does not take into account the altitude of trajectories here. In addition, we have used the mean of all trajectories in a cluster to represent that cluster.

We apply the Elbow criterion to determine the optimum number of clusters[38]. This heuristic method parameterizes the percentage of explained variance as a function of cluster count and chooses a number of clusters in such a way that adding another cluster does not increase the explained variance[39].

We have also calculated the probability of air mass transport from the stratosphere using 15 days back-trajectories. To determine the fraction of air mass coming from the stratosphere, we have counted the number of back-trajectories which traveled across the tropopause. The global tropopause analyses from NCEP is used for this purpose. While NCEP reanalyses, used in this

study, can resolve the synoptic-scale flow patterns, it is likely to provide underestimation of the actual Stratosphere-Troposphere Exchange (STE) occurrences and extension into the troposphere due to coarse temporal and spatial resolution[55].

Concentration weighted trajectory (CWT)

Since the analysis of the correlation between concentration at a measurement site and the backtrajectories gives much better information about where the source might be located along the path of the trajectory, we use one such methods in this study: Concentration weighted trajectory (CWT). CWT is a backward trajectories receptor model, which can be used for the determination of potential source areas of ozone at a receptor. It has the capability to determine the relative strength of potential sources by integrating ozone concentration at the receptor with back-trajectories[40].

CWT determines the average ozone concentration in a grid cell *ij* which is calculated as the normalized trajectory residence time weighted by the ozone concentration at the receptor location. Mathematically, CWT is estimated as follows:

$$CWT_{ij} = E(C_{ij}) = \frac{\sum_l C_{Rl}\tau_{ijl}}{\sum_l \tau_{ijl}} \quad (2)$$

where C_{ij} is the ozone concentration in a cell ij, C_{Rl} is the ozone concentration at the receptor for trajectory l and τ_{ijl} is the residence time of backward trajectories in cell *ij* for trajectory l.

CWT remedies the problem of false identification of potential sources near the receptor location by normalizing the source intensity of the grid cells with the trajectory residence time.

Multiple Receptors based CWT (MR-CWT)

Since we are examining a number of receptor locations in this study, a multi-site approach of CWT has been applied in order to take into account the spatial and temporal variabilities of all sites at once[41,42]. MR-CWT has advantages over single receptor CWT since the trailing effect may be eliminated and the most important potential source areas can be identified. This approach can help in identifying emission hotspots that have an impact on larger geographical scales.

MR-CWT has been calculated as follows:

$$MR\text{-}CWT_{ij} = \frac{\sum_k \sum_l C_{Rl}^k \tau_{ijl}^k}{\sum_k \sum_l \tau_{ijl}^k} \quad (3)$$

220 where C_{Rl}^{k} is the ozone concentration at k[th] receptor for trajectory l and τ_{ij}^{kl} is the residence time of
221 backward trajectories in cell ij corresponding to k[th] receptor for trajectory l.

222 **Weight function**

223 We apply an arbitrary weight function to receptor models (CWT) to reduce the uncertainties arising
224 from small number of trajectory end points in a grid cell. The weight function is given as follows
225 as[43] :

226 $$w(n_{ij}) = \begin{cases} 1.00, n_{ij} \geq 2N \\ 0.75, N \leq n_{ij} < 2N \\ 0.50{,}0.5N \leq n_{ij} < N \\ 0.25, n_{ij} < 0.5N \end{cases} \quad (4)$$

227 Here, n_{ij} is the number of end points in a grid cell *ij* and N is the average number of end points for
228 the whole study region. Weighted receptor models result in field gradient around the source region;
229 aiding in the identification of the potential sources.

230 **Trend estimation**

231 We calculate the trends using simple linear regression (SLR) for the time period. SLR is represented
232 as:

233 $$Y_t = c + xt + \epsilon_t$$
234 (5)

235 where c is the intercept and x is the trend (slope) of the line fitted using least square method.

236 To attribute the factors responsible for ozone variability, we also use the multiple linear regression
237 (MLR) based on least square minimization method[44] and Bayesian Dynamic linear model (DLM).
238 In the context of MLR, trend is defined as a change in the mean state of the system after all known
239 systematic effects, such as seasonality and long-term variabilities forced by external factors, have
240 been accounted for.

241 $$Y_t = c + xt + \sum_{n=1}^{2}\left(a_n cos(n\omega t) + b_n sin(n\omega t)\right) + \sum_i q_i F_i + \epsilon_t \quad (6)$$

242 where *t* is the number of months, *n* represents the seasonality of data (n=1 and n=2 accounts for
243 annual and half-yearly seasonality respectively) and $\omega = 2\pi/12$ for monthly sampled datasets.

We use MLR to explain variability in the tropospheric ozone time series using components for a constant mean level (represented by regression coefficient c) and a linear trend (x), for a seasonal effect (a_n and b_n), influence of external forcings (F), and for noise (ϵ) that is allowed to have autoregressive correlation. The autoregressive noise term accounts for long-range dependencies, irregular cycles, and the effects of different forcing mechanisms that a model could not capture. MLR uses autoregressive components of first order and seasons with annual and semi-annual components. Here, we include various proxies to account for the effects of different external forcings (both dynamical and chemical processes) that govern ozone change in the troposphere. These external drivers include solar radio flux (SF) at 10.7 cm wavelength as a representation for the solar cycle, heat flux (HF) at 200 hPa (averaged over 45–75 S) representing residual overturning circulation, potential vorticity (PV) at 200 hPa to account for the influence of polar vortex and stratosphere-troposphere mixing, aerosol optical depth (AOD) at 550 nm (averaged over 45–75 S) to account for volcanic eruptions, and AAO represents the mode of climate variability in southern high-latitudes, multivariate ENSO index (MEI) and QBO representing equatorial winds at 30 hPa and 50 hPa to account for influences of meteorological changes in the tropical region[9, 23, 56]. Heat flux at 200 hPa is calculated using ERA-Interim meteorology reanalyses from European Centre for Medium-Range Weather Forecasts (ECMWF) and AOD at 550 nm are from Modern-Era Retrospective analysis for Research and Applications, Version 2 (MERRA-2) reanalyses.

All proxies are deseasonlised by subtracting corresponding monthly climatological average and normalized over the period of study before being used for modeling. We calculate separate trends for monthly, annual and seasonal mean datasets with corresponding 95% confidence interval using both SLR and MLR (See supplementary material for discussion about DLM). We have checked for the multi-collinearity before performing trend estimation using variable influence factor (VIF)[50, 54]. The analysis suggests no multi-collinearity (VIF<10)[50] among included external forcings in this study (see Table S4).

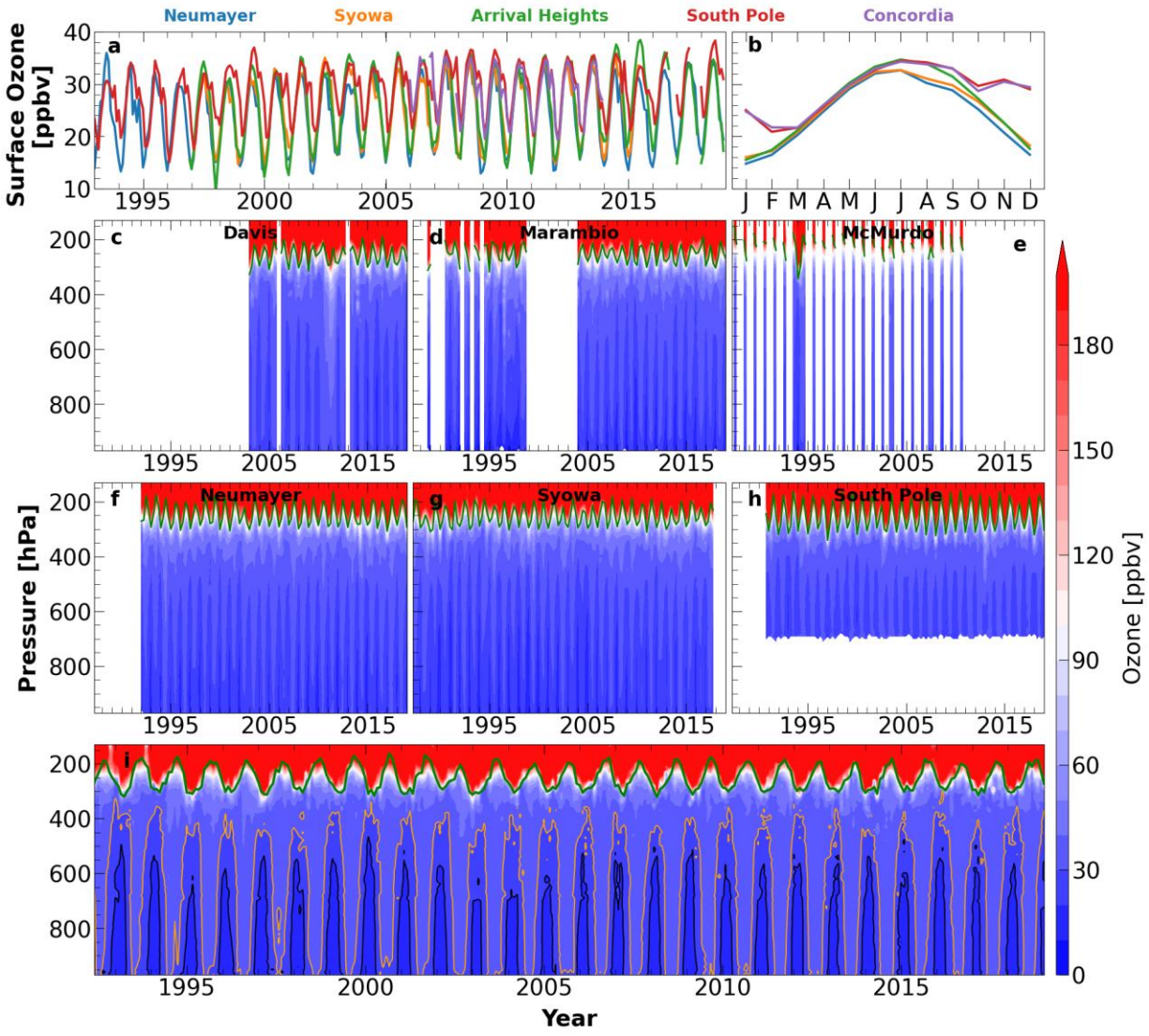

269

270 ***Figure 2:*** *(a) Temporal evolution of monthly averaged surface ozone at different stations (i.e.*
271 *Neumayer, Syowa, Arrival Heights, South Pole and Concordia), (b) Monthly climatology of surface*
272 *ozone and (c–h) seasonal average of ozone profiles. Here green lines show World Meteorological*
273 *Organization (WMO) defined thermodynamic tropopause pressure calculated using ozonesondes*
274 *temperature data. (i) Monthly weighted mean time-series of tropospheric ozone. Orange contours*
275 *show 30 ppbv and black contours show 20 ppbv ozone volume mixing ratio (vmr).*

RESULTS AND DISCUSSION

Surface and tropospheric ozone measurements

We have used all available surface ozone observations (1993–2018) and ozonesonde measurements (1987–2018) in Antarctica, which are shown in Fig. 2. Monthly time-series of surface ozone at various stations (Fig. 1) exhibits clear seasonal cycle, as depicted in Fig. 2 (a) with noticeable difference among the stations. While inland stations (South Pole and Concordia) have two annual peaks in surface ozone [one in winter (June-July-August; JJA) (~34 ppbv) and another in spring (September-October-November; SON) (~31 ppbv)], those in coastal regions have usually only one peak during winter (Fig. 2b). Among inland stations, South Pole encounters higher ozone values during peaks (up to 3 ppbv), but both South Pole and Concordia show similar minimum ozone values in February (20–22 ppbv). Inland stations are characterized by higher minimum values (~21 ppbv) during summer (December-January-February; DJF) than that of coastal stations (~15 ppbv).

Among the coastal stations, Arrival Heights show similar ozone values as that of inland stations during autumn (March-April-May; MAM) and winter seasons and are generally higher than other coastal stations as shown in Fig. 2 (b). Occurrence of high ozone concentration at Arrival Heights can be attributed to the katabatic winds that transport the ozone rich air mass from high altitude plateau. On the other hand, Neumayer and Syowa show analogous ozone concentration during autumn and winter, but the gap in the measured values between them becomes larger during spring and summer seasons; suggesting the transport of ozone-rich inland air mass to Syowa during these seasons. Seasonal cycle at both inland and coastal Antarctic sites are in accordance with our understanding about the remote regions with a maximum in winter season arising from accumulation of ozone transported from other regions and their photochemical destruction during spring and summer seasons[21]. Secondary peaks at inland stations in November-December arise as a result of the photochemical production from snow-pack emission of NO_x and synoptic scale air mass transport[25].

Fig. 2 (c–h) shows the time-series of seasonal mean tropospheric ozone (970–170 hPa) at different stations. The thick green lines show the variation of thermodynamic tropopause calculated using the World Meteorological Organization (WMO) definition[31]. The tropopause height and tropospheric ozone values are highly correlated with low ozone values when tropopause height is low (summer) and vice-versa; suggesting the influence of tropopause on ozone variability. Tropopause clearly shows the seasonal variation, which is largely controlled by the temperature difference between lower stratosphere and middle troposphere[45], as illustrated by 20 and 30 ppbv

ozone contours. The seasonal changes are influenced by the local meteorology and associated circulation changes, and stratosphere-troposphere exchange (STE) across the tropopause[4]. The STE normally occurs during tropopause folds caused by stratospheric polar vortex and mid-latitude synoptic scale disturbances[46] alongwith the forcing from below to fill the void caused by katabatic winds during winter[10].

Presence of measurement gaps and small sampling frequency for each month make the long-term analysis of individual station measurements meaningless, as the statistics will not be robust. Higher sampling can be achieved by regional aggregation of ozonesonde measurements from multiple stations located close to each other and sampling similar air masses. Regional aggregates are more representative for larger regions and permit the investigation of large-scale processes and their long-term evolution. Therefore, we calculate the weighted average[33] of all stations data accounting for the station type (inland or coastal) and ozonesonde uncertainties, and the same is shown in Fig. 2 (i). The time-series of monthly weighted mean at 970 hPa is depicted in Fig. S1 against the surface ozone at coastal stations.

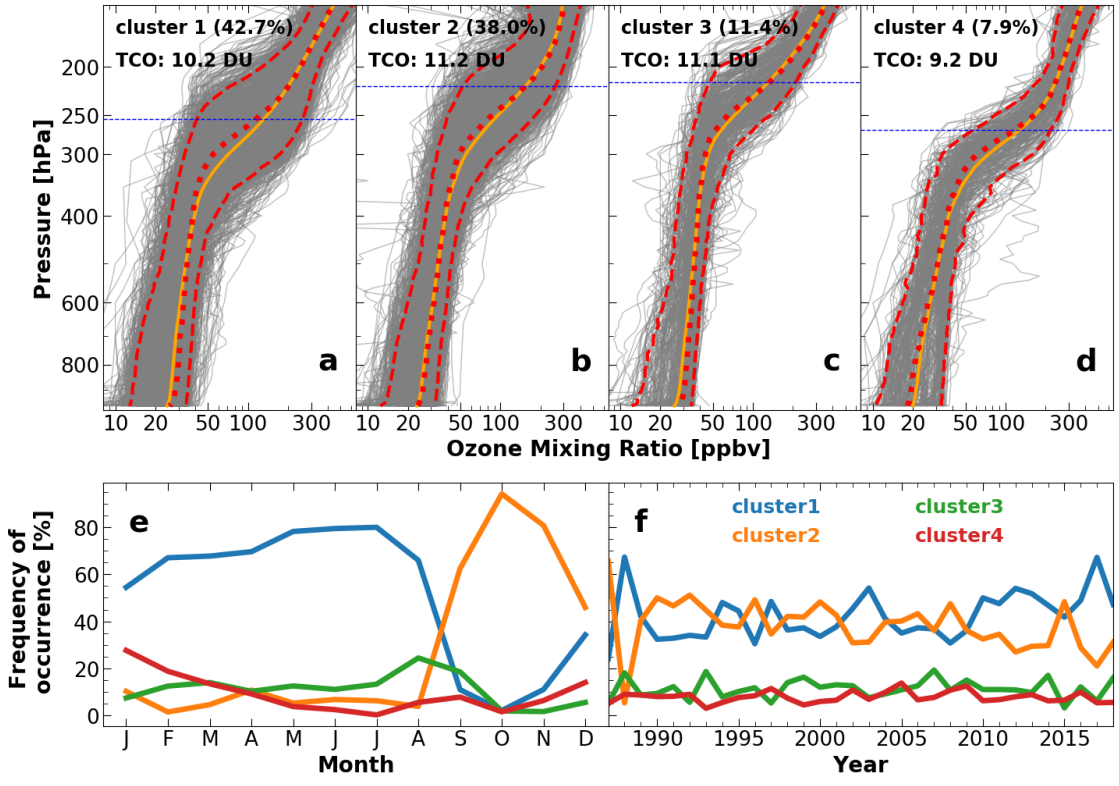

Figure 3: *(a–d) The SOM-based clusters of Antarctic ozone profiles upto 150 hPa. The orange solid lines represent the mean profiles of the cluster; red dotted lines represent median ozone profiles whereas 5th and 95th percentiles are shown in red dashed lines. Here, the blue lines show*

the mean tropopause pressure whereas TCO represents the mean tropospheric column ozone (in DU) for the given profile cluster. The (e) Monthly and (f) annual frequency of occurrences of clusters in the bottom panels.

Clustering of ozonesonde profiles

The variability of tropospheric ozone is assessed in detail using self-organizing map (SOM) based clusters of ozone profiles[47]. We find 4 different clusters (2 × 2 SOM nodes) of ozone from the lower troposphere to lower stratosphere (100 hPa) that are arranged in descending order according to the fraction of ozone profiles in clusters, as demonstrated in Fig. 3. See supplementary material for discussion about 9 (3 × 3) (Fig. S2) and 16 (4 × 4) (Fig. S3) SOM nodes. The lower stratosphere is also included in the analysis to capture the changes at the tropopause.

The cluster 1 represents the undisturbed ozone profiles (neither affected by depletion nor the enhancement episodes) with small mixing ratios in the troposphere and high values in the lower stratosphere. It is further characterized by lower tropopause height with high frequency of occurrence of the cluster in autumn and winter. Cluster 2 represents profiles with clear symptoms of ozone hole in the lower stratosphere and is characterized by moderate mixing ratios in the lower troposphere and higher tropopause height. It represents ozone profiles in spring and early summer with lower frequency in other seasons. Cluster 3 represents the profiles in late winter and early spring before the formation of ozone hole, and have the highest tropospheric ozone and tropopause altitude, which could be attributed to enhanced long-range transport from adjoining continents (Fig. S5) and STE (Fig. 11 of Hsu et al.[22]). As lower stratosphere is very cold, tropopause shifts upward during this period. On the other hand, cluster 4 represents profiles with the smallest ozone values in the lower troposphere, the lowest tropospheric column ozone and tropopause height, which occurs mostly during summer. Tropopause moves downward during summer due to warm stratosphere.

The cluster 2 has the highest tropospheric ozone column amount among all clusters. Since cluster 2 has almost all its profiles from spring season when tropopause height is lower than the winter months and the stratosphere-troposphere exchange is lowest (shown in Fig. 5 and also reported by Stohl et al.[48]), it suggests the occurrence of either the enhanced local ozone production / lower ozone loss in the troposphere or increased horizontal transport from the lower latitudes. As illustrated in Fig. 3, the ozone variability in Antarctica is dominated mainly by dynamical processes

associated with the changes in tropopause height and horizontal transport, which in turn determines the tropospheric ozone and its column amount. We further examine the long-term changes in the frequency of occurrence of various clusters. As depicted in Fig. 3 (f), cluster 2 clearly follows the evolution of stratospheric ozone during the study period with higher frequency in 1990s and smaller frequency in recent years[30], whereas the opposite is found in cluster 1 as it represents the background ozone. The clusters 3 and 4 show different temporal evolution with a clear reduction in frequency in recent years.

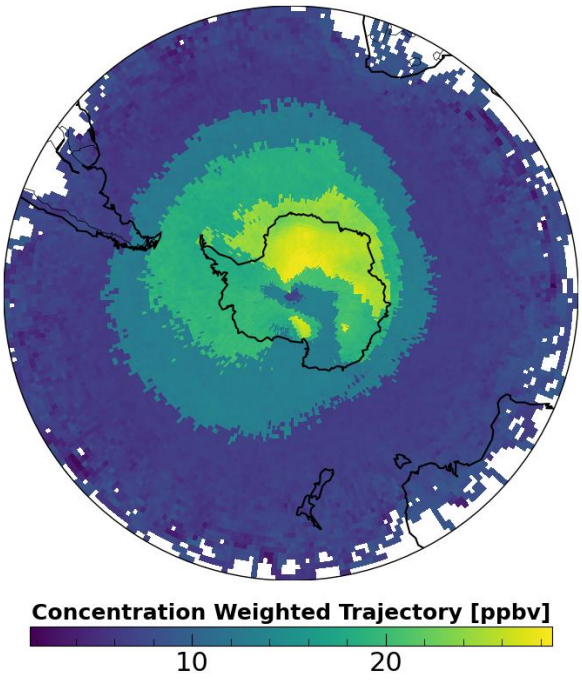

Figure 4: *Multiple Receptors based concentrated weighted trajectory (MR-CWT) for surface ozone based on 15 days backward trajectories at different stations calculated using HYSPLIT at 500 m.*

Air mass transport to Antarctica

As the analyses of surface ozone and ozone profiles suggest the dominance of seasonal variability driven by local meteorology and associated changes in synoptic-scale transport of air mass, we further investigate the changes in the air mass transport at various Antarctica stations with ozonesonde observations. There is only one study with such detailed air mass transport analysis over the Antarctic continent to date[48] and it examined the transport variability over 5.5 years (October 1999 – May 2005) only. However, we have studied air mass transport for more than 30 years (1987–2017). This is performed with 15-days backward trajectories calculated on daily basis

at several altitudes (e.g. 500, 1000, 5000, 8000, and 9000 m using the HYSPLIT model forced by NCEP meteorological reanalysis (2.5° latitude-longitude grids).

Fig. 4 shows the MR-CWT analysis for all 5 stations with surface ozone measurements. This analysis includes all available surface ozone measurements. As shown in Fig. 4, MR-CWT suggests that East Antarctic plateau is the most important source for surface ozone at stations under consideration. The marine area surrounding the continent is the second most important surface ozone source region; particularly the marine area near East Antarctic coasts. South America is also a significant source for surface ozone. Western Antarctic together with the Southern tip of South America, Scotia Sea, Amundsen Sea, Bellingshausen Sea and western part of Ross sea are also moderate sources; with areas in the foothills of Trans-Antarctic mountain in the Ross shelf region having surface ozone source potential as high as the East Antarctic regions. The trajectories corresponding to high ozone air masses travelled mostly over the high altitude inner part of the continent; consistent with the result of other studies conducted for the region [21,17].

The CWT analyses for individual stations show spatial features consistent with multi-receptors analysis, but there are discernible differences across stations and seasons (Fig. S4). For example, East Antarctica including Antarctic plateau and marine area very close to the East Antarctic coast are the major sources at South Pole. On the other hand, McMurdo station has sources distributed all around the Antarctic region throughout the year with major contributions from west Antarctica and Ross sea; barring the summer season when it is more concentrated over the Antarctic continent only. Stations based on East Antarctic coasts i.e. Syowa and Neumayer have similar sources. They are affected more by the marine area near to the coasts than other Antarctic based stations, but the Antarctic Plateau has sizeable contributions too. In contrast, Marambio has completely different sources than other stations, for which the air mass coming from South America and west Antarctica have major influence over the surface ozone variations. Antarctic continental regions (around 50% at 8000 m to 75% at 500 m) and the Ross Sea and the Weddel Sea (up to 15% at all altitudes) are the most frequent area of origin for 15-days backward trajectories (Fig. S5). The Southern American region has the highest contribution among the continents surrounding Antarctica (around 0.8% at 500 m to 2% in the upper troposphere). Australian region (including New Zealand) has a very small annual contribution in the lower troposphere (up to 0.2% at lower latitudes) but it increases with starting height (more than 2% at 8000 m). Sources over the continents show large monthly changes with the highest during the winter season (JJA) and the lowest during summer (DJF).

Fig. S6 depicts the clusters of back trajectories at various Antarctic-based stations and starting altitudes. The optimum number of trajectory clusters were determined using the Elbow method. The method suggests 5–7 clusters at different altitudes, but we have used 6 clusters at all stations and altitudes for consistency and ease of comparison. The transportation pathways can be divided roughly into 3 major categories: (i) fast moving long range eastward circumpolar transport along coasts characterized by transport from the southern ocean, (ii) poleward meridional transport accompanying the mid-latitude cyclones to the Antarctic coasts reaching even to the plateau, and (iii) the short range Katabatic outflow from the plateau to coasts especially to McMurdo[48]. The cyclones constitute the secondary circulation (poleward transport) over the Antarctic region with two main branches – one over the Tasman Sea area and other over the Weddell Sea area[17]. Among the routes, the outflow from the plateau is associated with the highest concentration of ozone, as it carries ozone-rich air mass usually coming from the UTLS, while circumpolar transport is generally associated with low ozone since it primarily carries air mass of marine origin or passes across coastal regions[21]. For example, the outflow from the plateau constitutes trajectory clusters with the lowest number of trajectories at 500 m in case of Neumayer (13%) and Syowa (11%). However, they are associated with the highest amount of average surface ozone concentration (25 ppbv and 27 ppbv respectively). The altitude of the mid-latitude trajectories is lower than that of the latitudes near Antarctica indicating the influence of near-surface air mass[51]. The transport from mid-latitude to Antarctica is generally facilitated by the globally highest frequency of cyclones over the seas around Antarctica. In general, the stations in the Antarctic Peninsula and the coastal regions of East Antarctica are affected by air mass transport from regions near South America, driven by synoptic atmospheric circulation patterns, which, in turn, are sensitive to different climate modes such as AAO and ENSO[52].

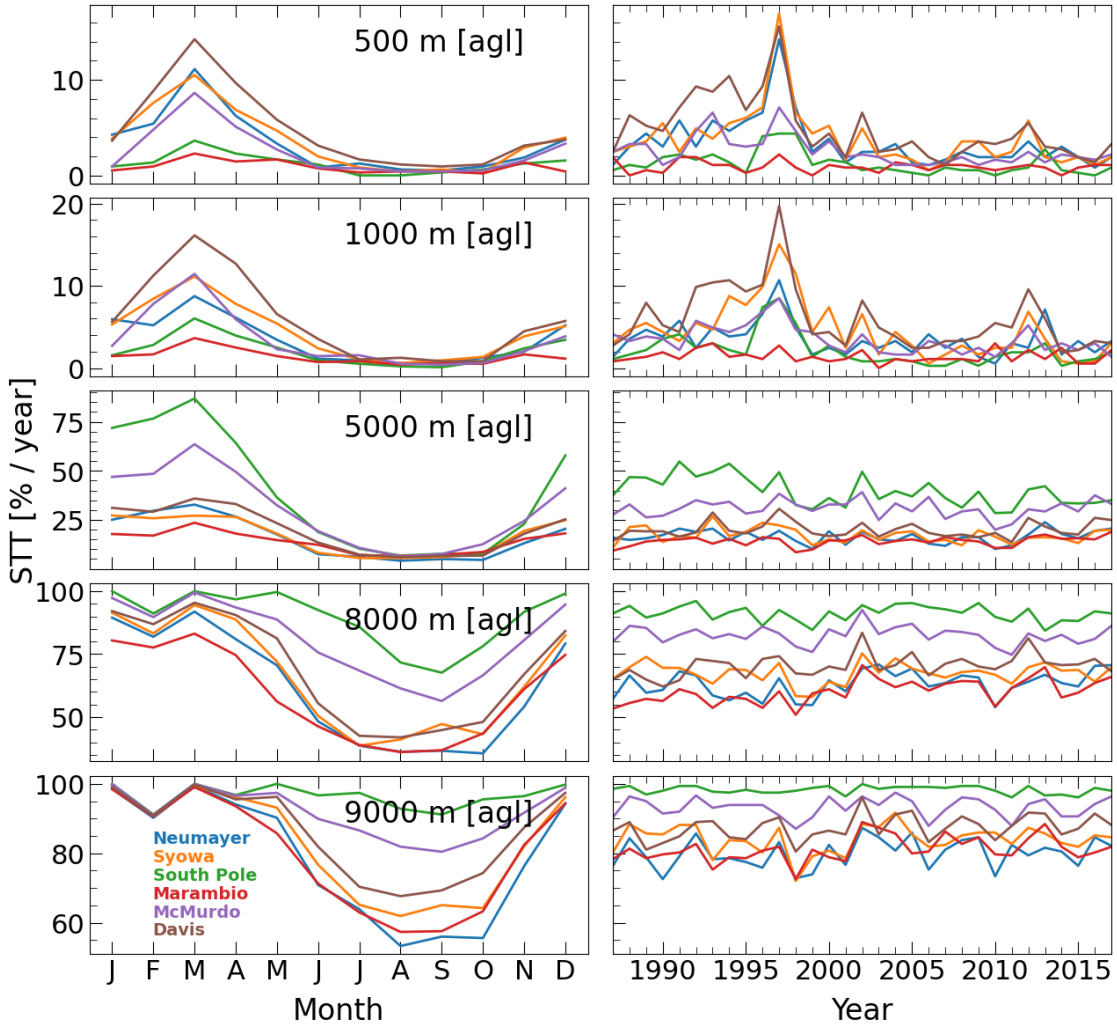

Figure 5: *(Left column) Monthly climatology and (right column) annual time-series of probability of stratosphere to troposphere transport (STT) within past 15 days for individual stations.*

Fig. 5 show the changes in probability of air mass transport from the stratosphere within last 15 days for all stations with ozonesonde measurements at different altitudes in the lower troposphere (500 and 1000 m, the middle troposphere (5000 m) and upper troposphere (8000 and 9000 m). While transport from stratosphere takes place throughout the year, there is large variations in horizontal transport across the months and seasons as shown in Fig. 5 (**left column**). The peak transport from stratosphere takes place during autumn season (March–April) in the lower (up to ~15%) and middle troposphere (~80%) and during both summer and autumn (up to 100%) in the upper troposphere, when the tropopause is at lower altitude at all stations, except at Marambio, which is situated in the Antarctic Peninsula. The minimum transport occurs in late winter and early spring due to the higher tropopause during the period. Marambio shows small variation in transport

444 across the months and seasons. South Pole station situated at the Antarctic Plateau receives the
445 most from stratosphere, but Marambio situated in Antarctic Peninsula receives the least. McMurdo
446 receives the largest portion of stratospheric air mass among all coastal stations. As it is situated in
447 Ross Ice Shelf region, it receives the coldest air due to katabatic winds[48]. We find even 100%
448 contribution from stratosphere in summer and autumn at 8000 and 9000 m, as the tropopause moves
449 below that altitude during this period.

450 While there is a consistent transport pattern across all altitudes with maximum in summer and
451 autumn, and minimum in winter, there exists a consistent steep vertical gradient, as also observed
452 by Stohl et al.[48]. Middle troposphere receives 5–10 times more transport from the stratosphere than
453 the lower troposphere. Downward transport to the troposphere from UTLS is facilitated by
454 intrusions in mid-latitude cyclones and residual mean flow driven by wave forcing in the
455 stratosphere[53]. Rossby wave breaking events, supported by mid-latitude cyclones on the poleward
456 side of the jet stream may detach air masses from the cyclonic circulation around the continent.
457 This facilitates a wave driven secondary circulation that transports air masses from the vortex edge
458 to the inner vortex, as observed over South Pole and McMurdo. Therefore, polar vortex modulated
459 long-range transport and downward transport from UTLS contribute significantly to the air masses
460 arriving at various stations in Antarctica.

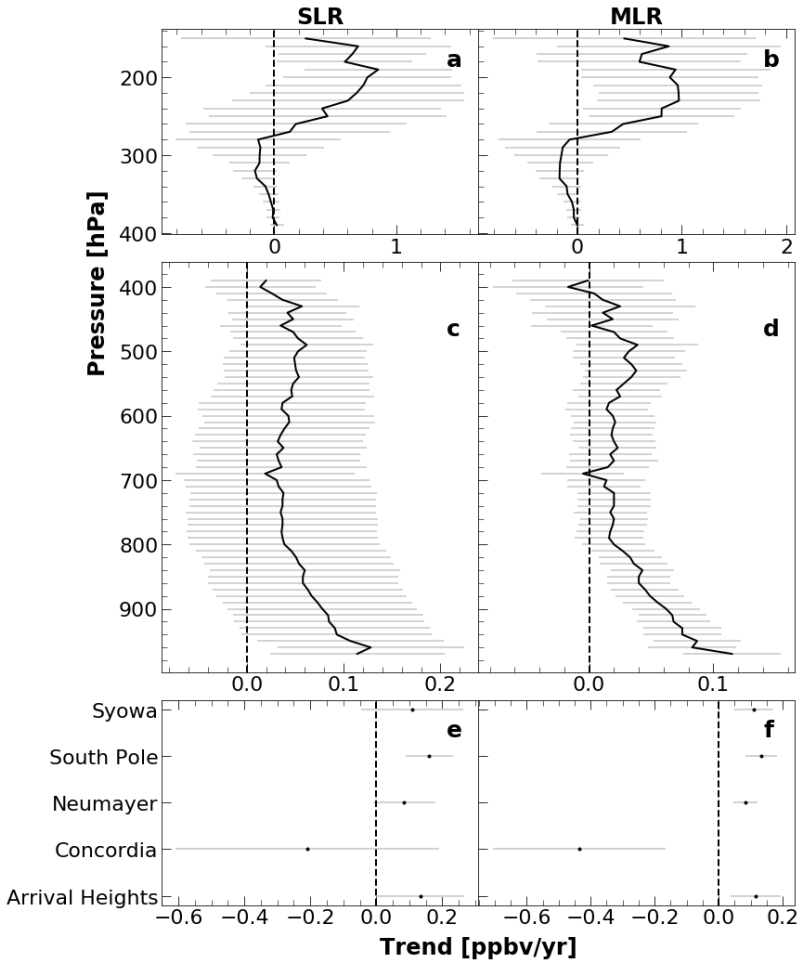

Figure 6: *Trends of monthly ozone data estimated using SLR and MLR. (a–d) solid black line shows the mean trend and gray error-bars show 95% confidence interval of estimated trends at different pressure levels. (e–f) black dots show the mean surface ozone trend at various stations and gray error-bars show 95% confidence interval of estimated trends. The trends are estimated in accordance with the availability of data at each station. The Arrival Heights surface ozone measurements are for the period 1997–2018, Concordia 2006–2013, Syowa 1997–2014, Neumayer 1993–2018, and South Pole 1993–2018.*

Tropospheric ozone trends

We first estimate the trend in tropospheric ozone using simple linear regression (SLR). We then calculate another long-term trend with multiple linear regression (MLR) that accounts for the contribution of various external drivers of ozone variability. In a recent study by Lu et al. [27], tropospheric ozone in the southern hemisphere was found to be influenced by the meridional

circulation which is, in turn, driven by momentum deposition of atmospheric waves propagating from the troposphere as well as diabatic heating by radiative processes dependent on the concentration of stratospheric CO_2 and ozone in Antarctica. The long-term evolution of the meridional circulation has been studied extensively and found to be affected by several interannual variabilities such as Southern Annular Mode (SAM), ENSO, QBO, Pacific Decadal Oscillation (PDO) and solar cycle. El Niño / easterly shear QBO act to strengthen the stratospheric overturning circulation and hence the downward transport to the troposphere (particularly during winter) whereas La Niña / westerly shear QBO is associated with weakened circulation and decreased transport to the troposphere[23]. Therefore, we include ENSO, QBO, SF, AAO, AOD, HF and PV as the potential drivers of tropospheric ozone variability in Antarctica (see Methods).

Trends calculated with monthly average datasets using SLR and MLR are displayed in Fig. 6 (a–d), and Fig. S7–8 (a–d) show the same with 95% confidence interval using annual and seasonal data (See supplementary material for analysis using DLM). While SLR of monthly and annual data show increasing ozone trends in the lower and middle troposphere up to 400 hPa (0.02–0.13 ppbv/year), only the trends in the lower troposphere are significant at 95% confidence interval (up to 950 hPa in case of monthly data and 800 hPa in case of annual data). Trends are about 0.01–0.12 ppbv/year for both monthly and annually averaged ozone profiles. On the other hand, ozone trends in autumn (MAM) show significant positive trends up to 400 hPa and are the largest among all seasonal trends (0.06–0.13 ppbv/year). The smallest trends are found in spring (SON; less than -0.03 ppbv/year), but are insignificant. Both monthly and annual data show insignificant negative trends (up to -0.18 ppbv/year) at 400–280 hPa and positive trends (up to 0.9 ppbv/year) above the altitude 280 hPa. All seasonal data tend to follow similar insignificant negative trends between 400 and 280 hPa. However, they differ in altitudes above 280 hPa with positive trends in spring and summer.

When compared to the trends computed using the SLR method, the monthly data show similar positive trends in the lower and middle troposphere up to 400 hPa in the MLR analyses too, and the trends are significant up to 800 hPa (0.02–0.12 pbv/year). However, the annual data show positive trends only in the lower troposphere below 580 hPa (up to 0.14 ppbv/year) and is negative above 400 hPa. The trend estimates for all seasons, except spring, show insignificant but positive trends in the lower and mid-troposphere up to 400 hPa, although a few sporadic digression to negative values at some altitudes (near 700 and 800 hPa). Spring ozone profiles show positive trends at altitudes below 850 hPa (up to 0.2 ppbv/year) and negative trends at 850–280 hPa (up to -0.18 ppbv/year). In the upper troposphere, the monthly data show trends similar to that of SLR,

but the annual MLR digress from that of SLR above 200 hPa and are smaller compared to the SLR trends. The MLR analyses with the seasonal data show trends very similar to that estimated with SLR in the upper troposphere. In sum, the tropospheric trends are positive at pressure levels above 400 hPa; suggesting significant ozone pollution in Antarctica.

Table S2 summarises the surface ozone trend whereas Fig. 6 (e–f) and Fig. S7–8 (e–f) show the same with 95% confidence interval estimated with the SLR and MLR methods. Due to short time period (7 years of available data) at Concordia, we have excluded the trend analyses with seasonal and annual observations for Concordia. Model fit for MLR are shown in Fig. S10. MLR reproduces the observed data very well (R^2 ranges from 0.864 at South Pole to 0.957 at Syowa), although R^2 is smaller for South Pole and Concordia measurements due to the presence of secondary ozone peaks in November/December. Both methods show positive trends at all stations (up to 0.16 ppbv/year in SLR and 0.13 ppbv/year in MLR) except Concordia (-0.2 ppbv/year in SLR and -0.44 ppbv/year in MLR) estimated using the monthly data. The SLR trends for monthly data are insignificant at 95% confidence interval for all stations except at South Pole (0.16 ppbv/year) and Arrival Heights (0.13 ppbv/year). However, they are significant for all stations with MLR. Despite of the differences in methodology adopted, SLR trends for Neumayer (0.08 ± 0.05 ppbv/year) and South Pole (0.16 ± 0.04 ppbv/year) are in agreement with those reported by Cooper et al. (2020)[17] ie. 0.10 ± 0.04 ppbv/year and 0.15 ± 0.06 ppbv/year respectively. Negative trend at Concordia during 2006–2013 is consistent with negative but insignificant trend at the South Pole station during the same period. The trends estimated using the annual average data by both SLR (up to 0.146 ppbv/year) and MLR (up to 0.098 ppbv/year) are positive for all stations, but they are significant as analysed with SLR and insignificant with MLR (except Neumayer). The seasonal data tend to follow the similar trend as monthly data for SLR and MLR (except South Pole in summer) and are mostly insignificant by MLR. The analyses with autumn data show the largest trend (0.22 ppbv/year) among the seasons for SLR[46]. Although all stations show positive trends over the considered time period, the rate of increase has reduced in recent years with Arrival Heights showing negative trends after 2015, as shown in Fig. S11 (analysed using DLM).

Fig. S11 (e) shows the temporal evolution and Fig. S11 (f) depicts trend of monthly mean TCO estimated using DLM, whereas Table S2 lists the trends estimated with SLR and MLR. The TCO is calculated by integrating individual ozone profiles up to the thermodynamic tropopause. The SLR trend show positive values for the monthly (0.005 DU/year), summer (DJF; 0.004 DU/year) and autumn (MAM; 0.031 DU/year) seasons, although they are significant only in autumn. Similarly, the MLR analyses show positive trends in summer (0.001 DU/year) and autumn (0.024

DU/year) with statistically significant values in autumn. All other data show insignificant but negative trends. The DLM analysis for monthly data show insignificant trends.

Contribution of Forcings to tropospheric ozone variability

Fig. S12 shows the contribution of proxies to ozone variability at 100–900 hPa. The regression coefficients are multiplied by the value of each proxy to estimate the contribution to ozone changes and are scaled by the cumulative contributions from all proxies for percentage contributions. It reveals that HF (33%) accounts for most of the variability followed by QBO (25%), AAO (20%), PV (16%), MEI (12%), and SF (11%). AOD is a prominent contributor in the mid-troposphere (11%). The analyses clearly demonstrate the dynamical control of tropospheric ozone in Antarctica. It suggests that the variations in stratosphere-troposphere exchange due to changes in residual circulation represented by HF and changes in the strength of the polar vortex represented by PV account for most of the inter-annual variability in tropospheric ozone with sizable contributions attributable to tropical teleconnections and southern annular mode represented by AAO[54].

Table S3 summarizes the contributions of proxies to inter-annual surface ozone variability. Contributions vary significantly across the stations with the largest contributions from HF (78%) followed by AAO (21%), QBO (18%), SF (15%), and PV (11%). AOD and MEI have contributions less than 7% at all stations, and HF predominately affects the coastal stations, whereas QBO mostly influences the inland stations. The analyses thus demonstrate that the variability of surface ozone is primarily regulated by atmospheric dynamics represented by the heat flux and polar vortex. The assessment also reveals that the tropical teleconnections and southern oscillation have a substantial effect on the surface ozone variability in Antarctica, as shown in the case of tropospheric ozone.

The assessment of the tropospheric ozone column (Table S3) shows that AAO (21%) is the largest contributor to inter-annual ozone variability, and is followed by the contributions from QBO (18%), HF (12%), PV (11%) and SF (11%). It is interesting to note the contributions from MEI, which is about 5% and is smaller than the contributions from other proxies; suggesting a negligible influence of ENSO on the ozone column variability there. As discussed for surface ozone and tropospheric ozone profiles, the contributions of HF, AAO, and QBO are also very important in the column changes.

In summary, the study of tropospheric ozone trends in remote locations like Antarctica is limited by the dearth of ground-based ozonesondes measurements due to inhospitable conditions and extreme remoteness. Additionally, the available measurements have a huge amount of missing data; rendering inappropriate the station-wise trend analysis. Therefore, we have compiled a tropospheric ozone dataset from all available ozonesondes measurements accounting for the differences among various stations and their uncertainties. The analysis of clusters reveals the predominance of tropopause height on the clusters. Ozone in the upper troposphere and lower stratosphere drives the clustering at these Antarctic-based stations. The analysis identifies the Antarctic plateau as the most dominant source region especially in the summer season for near-surface ozone; complemented by long-range transport especially from the Southern tip of the South American continent in the lower troposphere. Furthermore, transport from the stratosphere also contributes significantly to the tropospheric ozone even in the lower troposphere.

Atmospheric ozone shows an increasing trend in the lower and middle troposphere, but a decreasing trend in the upper troposphere over the period. Meanwhile, the analysis of the surface ozone measurements corroborates this increasing ozone trend shown by the ozonesondes in the lower troposphere. The increasing trend is significant even after accounting for natural variability arising from intra- and inter-annual processes; suggesting rising ozone values in Antarctica. This increasing trend may be due to increased emissions from neighboring continents, tourist visits to Antarctica[57] and other modes of climate variabilities; not accounted for in this study. As the tropospheric ozone has a positive feedback relationship with global warming, it surfaces a serious concern about the change in climate in the Antarctic region. Consequently, this change in the Antarctic climate would have important long-term implications, such as the melting sea-ice, changes in water mass, and negative impacts on the ecosystem.

ASSOCIATED CONTENT

Supplementary Information

The Supporting Information is available free of charge on the ACS Publications website.

Conflict of Interest

We wish to confirm that there are no known conflicts of interest associated with this publication and there has been no significant financial support for this work that could have influenced its outcome.

ACKNOWLEDGMENTS

We thank the Head CORAL, and the Director IIT Kharagpur for facilitating the study. We would like to acknowledge PNRA Projects **DO3meCO2**, **ABL-CLIMAT** and **LTCPAA** for funding the experimental activities at WMO/GAW Concordia. We would like to thank all ozonesonde and ground-based stations data teams and their respective government/funding agencies. Ozonesonde data are publicly available from NDACC and WOUDC. We thank the ECMWF, MERRA2 (NASA) and NCEP data providers for making them available for this study. We thank the Department of Science and Technology (DST), Ministry of Human Resource Development (MHRD), Indian Institute of Technology Kharagpur (IIT KGP), , National Centre for Ocean Information Services (INCOIS), Hyderabad and Ministry of Earth Science (MoES) for facilitating and funding (O–MASCOT project) the study. We also thank all the data managers and the scientists who made available those data for this study. We thank Dr. M. Ravichandran, Director, National Centre for Ocean and Polar Research Goa, India for his encouragement and support for this study.

REFERENCES

(1) WMO (World Meteorological Organization). Scientific assessment of ozone depletion: 2006. *Global Ozone Research and Monitoring Project-Report No. 50* **2007**.

(2) Gaudel, A.; Cooper, O. R.; Ancellet, G.; Barret, B.; Boynard, A.; Burrows, J. P.; Clerbaux, C.; Coheur, P.-F.; Cuesta, J.; Cuevas, E.; Doniki, S.; Dufour, G.; Ebojie, F.; Foret, G.; Garcia, O.; Granados-Muñoz, M. J.; Hannigan, J. W.; Hase, F.; Hassler, B.; Huang, G.; Hurtmans, D.; Jaffe, D.; Jones, N.; Kalabokas, P.; Kerridge, B.; Kulawik, S.; Latter, B.; Leblanc, T.; Le Flochmoën, E.; Lin, W.; Liu, J.; Liu, X.; Mahieu, E.; Mcclure-Begley, A.; Neu, J. L.; Osman, M.; Palm, M.; Petetin, H.; Petropavlovskikh, I.; Querel, R.; Rahpoe, N.; Rozanov, A.; Schultz, M. G.; Schwab, J.; Siddans, R.; Smale, D.; Steinbacher, M.; Tanimoto, H.; Tarasick, D. W.; Thouret, V.; Thompson, A. M.; Trickl, T.; Weatherhead, E.; Wespes, C.; Worden, H. M.; Vigouroux, C.; Xu, X.; Zeng, G.; Ziemke, J. Tropospheric Ozone Assessment Report: Present-day distribution and trends of tropospheric ozone relevant to climate and global atmospheric chemistry model evaluation Tropospheric Ozone Assessment Report: Present-day distribution and trends of tropospheric. *Elementa: Science of the Anthropocene* **2018,** 6.

(3) Pommier, M.; Fagerli, H.; Gauss, M.; Simpson, D.; Sharma, S.; Sinha, V.; Ghude, S. D.; Landgren, O.; Nyiri, A.; Wind, P. Impact of regional climate change and future emission scenarios

on surface O 3 and PM 2.5 over India. *Atmospheric Chemistry and Physics* **2018**, *185194*, 103–127.

(4) Greenslade, J. W.; Alexander, S. P.; Schofield, R.; Fisher, J. A.; Klekociuk, A. K. Stratospheric ozone intrusion events and their impacts on tropospheric ozone in the Southern Hemisphere. *Atmospheric Chemistry and Physics* **2017**, *17* (17), 10269–10290.

(5) Fleming, Z. L.; Doherty, R. M.; Von Schneidemesser, E.; Malley, C. S.; Cooper, O. R.; Pinto, J. P.; Colette, A.; Xu, X.; Simpson, D.; Schultz, M. G.; Lefohn, A. S.; Hamad, S.; Moolla, R.; Solberg, S.; Feng, Z. Tropospheric ozone assessment report: Present-day ozone distribution and trends relevant to human health. *Elementa: Science of the Anthropocene* **2018**, *6* (1), 12.

(6) Han, H.; Liu, J.; Yuan, H.; Zhuang, B.; Zhu, Y.; Wu, Y.; Yan, Y.; Ding, A. Characteristics of intercontinental transport of tropospheric ozone from Africa to Asia. *Atmospheric Chemistry and Physics* **2018**, *18* (6), 4251–4276.

(7) Hess, P. G.; Zbinden, R. Stratospheric impact on tropospheric ozone variability and trends: 1990-2009. *Atmospheric Chemistry and Physics* **2013**, *13*, 649–674.

(8) Lin, M.; Horowitz, L. W.; Oltmans, S. J.; Fiore, A. M.; Fan, S. Tropospheric ozone trends at Mauna Loa Observatory tied to decadal climate variability. *Nature Geoscience* **2014**, *7* (2), 136–143.

(9) Wespes, C.; Hurtmans, D.; Clerbaux, C.; Coheur, P.-F. O3 variability in the troposphere as observed by IASI over 2008-2016: Contribution of atmospheric chemistry and dynamics. *Journal of Geophysical Research: Atmospheres* **2017**, *122* (4), 2429–2451.

(10) Roscoe, H. K. Possible descent across the “Tropopause” in Antarctic winter. *Advances in Space Research* **2004**, *33* (7), 1048–1052.

(11) Screen, J. A.; Bracegirdle, T. J.; Simmonds, I. Polar Climate Change as Manifest in Atmospheric Circulation. *Current Climate Change Reports* **2018**, *4* (4), 383–395.

(12) Calvo, N.; Polvani, L. M.; Solomon, S. On the surface impact of Arctic stratospheric ozone extremes. *Environmental Research Letters* **2015**, *10* (9), 094003.

(13) Cooper, O. R.; Parrish, D. D.; Ziemke, J.; Balashov, N. V.; Cupeiro, M.; Galbally, I. E.; Gilge, S.; Horowitz, L.; Jensen, N. R.; Lamarque, J.-F.; Naik, V.; Oltmans, S. J.; Schwab, J.; Shindell, D. T.; Thompson, A. M.; Thouret, V.; Wang, Y.; Zbinden, R. M. Global distribution and trends of

tropospheric ozone: An observation-based review. *Elementa: Science of the Anthropocene* **2014**, *2*, 000029.

(14) Zeng, G.; Morgenstern, O.; Shiona, H.; Thomas, A. J.; Querel, R. R.; Nichol, S. E. Attribution of recent ozone changes in the Southern Hemisphere mid-latitudes using statistical analysis and chemistry–climate model simulations. *Atmospheric Chemistry and Physics* **2017**, *17* (17), 10495–10513.

(15) Hu, L.; Jacob, D. J.; Liu, X.; Zhang, Y.; Zhang, L.; Kim, P. S.; Sulprizio, M. P.; Yantosca, R. M. Global budget of tropospheric ozone: Evaluating recent model advances with satellite (OMI), aircraft (IAGOS), and ozonesonde observations. *Atmospheric Environment* **2017**, *167*, 323–334.

(16) Cooper, O. R.; Schultz, M. G.; Schröder, S.; Chang, K.-L.; Gaudel, A.; Benítez, G. C.; Cuevas, E.; Fröhlich, M.; Galbally, I. E.; Molloy, S.; Kubistin, D.; Lu, X.; McClure-Begley, A.; Nédélec, P.; O'Brien, J.; Oltmans, S. J.; Petropavlovskikh, I.; Ries, L.; Senik, I.; Sjöberg, K.; Solberg, S.; Spain, G. T.; Spangl, W.; Steinbacher, M.; Tarasick, D.; Thouret, V.; Xu, X. Multi-decadal surface ozone trends at globally distributed remote locations. *Elementa: Science of the Anthropocene* **2020**, *8* (1), 23.

(17) Masclin, S.; Frey, M. M.; Rogge, W. F.; Bales, R. C. Atmospheric nitric oxide and ozone at the WAIS Divide deep coring site: a discussion of local sources and transport in West Antarctica. *Atmospheric Chemistry and Physics* **2013**, *13* (17), 8857–8877.

(18) Young, P. J.; Naik, V.; Fiore, A. M.; Gaudel, A.; Guo, J.; Lin, M. Y.; Neu, J. L.; Parrish, D. D.; Rieder, H. E.; Schnell, J. L.; Tilmes, S.; Wild, O.; Zhang, L.; Ziemke, J. R.; Brandt, J.; Delcloo, A.; Doherty, R. M.; Geels, C.; Hegglin, M. I.; Hu, L.; Im, U.; Kumar, R.; Luhar, A.; Murray, L.; Plummer, D.; Rodriguez, J.; Saiz-Lopez, A.; Schultz, M. G.; Woodhouse, M. T.; Zeng, G. Tropospheric Ozone Assessment Report: Assessment of global-scale model performance for global and regional ozone distributions, variability, and trends. *Elementa: Science of the Anthropocene* **2018**, *6* (1), 10.

(19) Cristofanelli, P.; Bonasoni, P.; Calzolari, F.; Bonafè, U.; Lanconelli, C.; Lupi, A.; Trivellone, G.; Vitale, V.; Petkov, B. Analysis of near-surface ozone variations in Terra Nova Bay, Antarctica. *Antarctic Science* **2008**, *20* (4), 415–421.

(20) Helmig, D.; Oltmans, S. J.; Carlson, D.; Lamarque, J.-F.; Jones, A.; Labuschagne, C.; Anlauf, K.; Hayden, K. A review of surface ozone in the polar regions. *Atmospheric Environment* **2007**, *41* (24), 5138–5161.

(21) Legrand, M.; Preunkert, S.; Savarino, J.; Frey, M. M.; Kukui, A.; Helmig, D.; Jourdain, B.; Jones, A. E.; Weller, R.; Brough, N.; Gallée, H. Inter-annual variability of surface ozone at coastal (Dumont d'Urville, 2004–2014) and inland (Concordia, 2007–2014) sites in East Antarctica. *Atmospheric Chemistry and Physics* **2016**, *16* (12), 8053–8069.

(22) Hsu, J.; Prather, M. J. Stratospheric variability and tropospheric ozone. *Journal of Geophysical Research Atmospheres* **2009**, *114* (6), D06102.

(23) Neu, J. L.; Flury, T.; Manney, G. L.; Santee, M. L.; Livesey, N. J.; Worden, J. Tropospheric ozone variations governed by changes in stratospheric circulation. *Nature Geoscience* **2014,** *7*(5), 340–344.

(24) Anet, J. G.; Steinbacher, M.; Gallardo, L.; Velásquez Álvarez, P. A.; Emmenegger, L.; Buchmann, B. Surface ozone in the Southern Hemisphere: 20 years of data from a site with a unique setting in El Tololo, Chile. *Atmospheric Chemistry and Physics* **2017**, *17* (10), 6477–6492.

(25) Cristofanelli, P.; Putero, D.; Bonasoni, P.; Busetto, M.; Calzolari, F.; Camporeale, G.; Grigioni, P.; Lupi, A.; Petkov, B.; Traversi, R.; Udisti, R.; Vitale, V. Analysis of multi-year near-surface ozone observations at the WMO/GAW "Concordia" station (75°06′S, 123°20′E, 3280 m a.s.l. – Antarctica). *Atmospheric Environment* **2018**, *177* (December 2017), 54–63.

(26) Zhang, Y.; Cooper, O. R.; Gaudel, A.; Thompson, A. M.; Nédélec, P.; Ogino, S.-Y.; West, J. J. Tropospheric ozone change from 1980 to 2010 dominated by equatorward redistribution of emissions. *Nature Geoscience 2016 9:12* **2016**, *9* (12), 875.

(27) Lu, X.; Zhang, L.; Zhao, Y.; Jacob, D. J.; Hu, Y.; Hu, L.; Gao, M.; Liu, X.; Petropavlovskikh, I.; McClure-Begley, A.; Querel, R. Surface and tropospheric ozone trends in the Southern Hemisphere since 1990: possible linkages to poleward expansion of the Hadley circulation. *Science Bulletin* **2019**, *64* (6), 400–409.

(28) Mills, G.; Pleijel, H.; Malley, C. S.; Sinha, B.; Cooper, O. R.; Schultz, M. G.; Neufeld, H. S.; Simpson, D.; Sharps, K.; Feng, Z.; Gerosa, G.; Harmens, H.; Kobayashi, K.; Saxena, P.; Paoletti, E.; Sinha, V.; Xu, X. Tropospheric Ozone Assessment Report: Present-day tropospheric ozone distribution and trends relevant to vegetation. *Elementa: Science of the Anthropocene* **2018**, *6* (47).

(29) Chang, K.-L.; Cooper, O. R.; Gaudel, A.; Petropavlovskikh, I.; Thouret, V. Statistical regularization for trend detection: an integrated approach for detecting long-term trends from sparse tropospheric ozone profiles. *Atmospheric Chemistry and Physics* **2020**, *20* (16), 9915–9938.

(30) Kuttippurath, J.; Kumar, P.; Nair, P. J.; Pandey, P. C. Emergence of ozone recovery evidenced by reduction in the occurrence of Antarctic ozone loss saturation. *npj Climate and Atmospheric Science* **2018**, *1* (1), 42.

(31) Wilcox, L. J.; Hoskins, B. J.; Shine, K. P. A global blended tropopause based on ERA data. Part I: Climatology. *Quarterly Journal of the Royal Meteorological Society* **2012**, *138* (664), 561–575.

(32) Spencer, C. J.; Yakymchuk, C.; Ghaznavi, M. Visualising data distributions with kernel density estimation and reduced chi-squared statistic. *Geoscience Frontiers* **2017**, *8* (6), 1247–1252.

(33) Martinez, M.; Bartholomew, M. What Does It "Mean"? A Review of Interpreting and Calculating Different Types of Means and Standard Deviations. *Pharmaceutics* **2017**, *9* (4), 14.

(34) Stauffer, R. M.; Thompson, A. M.; Young, G. S. Tropospheric ozonesonde profiles at long-term U.S. monitoring sites: 1. A climatology based on self-organizing maps. *Journal of Geophysical Research: Atmospheres* **2016**, *121* (3), 1320–1339.

(35) Warner, M. S. C. Introduction to PySPLIT: A Python Toolkit for NOAA ARL's HYSPLIT Model. *Computing in Science & Engineering* **2018**, *20* (5), 47–62.

(36) Stein, A. F.; Draxler, R. R.; Rolph, G. D.; Stunder, B. J. B.; Cohen, M. D.; Ngan, F.; Stein, A. F.; Draxler, R. R.; Rolph, G. D.; Stunder, B. J. B.; Cohen, M. D.; Ngan, F. NOAA's HYSPLIT Atmospheric Transport and Dispersion Modeling System. *Bulletin of American Meteorological Society* **2015**, *96* (12), 2059–2077.

(37) Nawaz, T.; Cavallaro, A.; Rinner, B. Trajectory clustering for motion pattern extraction in aerial videos. In *2014 IEEE International Conference on Image Processing (ICIP)*; IEEE, 2014; pp 1016–1020.

(38) Novikov, A. PyClustering: Data Mining Library. *Journal of Open Source Software* **2019**, *4* (36), 1230.

(39) Shao, J.; Tanner, S. W.; Thompson, N.; Cheatham, T. E. Clustering Molecular Dynamics Trajectories: 1. Characterizing the Performance of Different Clustering Algorithms. *Journal of Chemical Theory and Computation* **2007**, *3* (6), 2312–2334.

(40) Brereton, C. A.; Johnson, M. R. Identifying sources of fugitive emissions in industrial facilities using trajectory statistical methods. *Atmospheric Environment* **2012**, *51*, 46–55.

(41) Han, Y. J.; Holsen, T. M.; Hopke, P. K. Estimation of source locations of total gaseous mercury measured in New York State using trajectory-based models. *Atmospheric Environment* **2007**, *41* (28), 6033–6047.

(42) Petit, J.-E.; Favez, O.; Albinet, A.; Canonaco, F. A user-friendly tool for comprehensive evaluation of the geographical origins of atmospheric pollution: Wind and trajectory analyses. *Environmental Modelling & Software* **2017**, *88*, 183–187.

(43) Stojić, A.; Stanišić Stojić, S. The innovative concept of three-dimensional hybrid receptor modeling. *Atmospheric Environment* **2017**, *164*, 216–223.

(44) Kuchar, A.; Ball, W. T.; Rozanov, E. V.; Stenke, A.; Revell, L.; Miksovsky, J.; Pisoft, P.; Peter, T. On the aliasing of the solar cycle in the lower stratospheric tropical temperature. *Journal of Geophysical Research: Atmospheres* **2017**, *122* (17), 9076–9093.

(45) Zängl, G.; Hoinka, K. P. The Tropopause in the Polar Regions. *Journal of Climate* **2001**, *14* (14), 3117–3139.

(46) Sprenger, M. Tropopause folds and cross-tropopause exchange: A global investigation based upon ECMWF analyses for the time period March 2000 to February 2001. *Journal of Geophysical Research* **2003**, *108* (D12), 1–11.

(47) Stauffer, R. M.; Thompson, A. M.; Witte, J. C. Characterizing Global Ozonesonde Profile Variability From Surface to the UT/LS With a Clustering Technique and MERRA-2 Reanalysis. *Journal of Geophysical Research: Atmospheres* **2018**, *123* (11), 6213–6229.

(48) Stohl, A.; Sodemann, H. Characteristics of atmospheric transport into the Antarctic troposphere. *Journal of Geophysical Research Atmospheres* **2010**, *115* (D2), 1–16.

(49) Hara, K.; Sudo, K.; Ohnishi, T.; Osada, K.; Yabuki, M.; Shiobara, M.; Yamanouchi, T. Seasonal features and origins of carbonaceous aerosols at Syowa Station, coastal Antarctica. *Atmospheric Chemistry and Physics* **2019**, *19* (11), 7817–7837.

(50) Estrada-Peña, A.; Estrada-Sánchez, A.; Estrada-Sánchez, D.; Fuente, J. de la. Assessing the effects of variables and background selection on the capture of the tick climate niche. *International Journal of Health Geographics* **2013**, 12, 1–13.

(51) Ahn, D. H.; Choi, T.; Kim, J.; Park, S. S.; Lee, Y. G.; Kim, S.-J.; Koo, J.-H. Southern Hemisphere mid- and high-latitudinal AOD, CO, NO2, and HCHO: spatiotemporal patterns revealed by satellite observations. *Progress in Earth and Planetary Science* **2019**, *6* (1), 34.

(52) Gonzalez, S.; Vasallo, F.; Recio-Blitz, C.; Guijarro, J. A.; Riesco, J. Atmospheric patterns over the Antarctic Peninsula. *Journal of Climate* **2018**, *31* (9), 3597–3608.

(53) Hirano, S.; Kohma, M.; Sato, K. A three-dimensional analysis on the role of atmospheric waves in the climatology and interannual variability of stratospheric final warming in the Southern Hemisphere. *Journal of Geophysical Research* **2016**, *121* (14), 8429–8443.

(54) Hasyim, H.; Nursafingi, A.; Haque, U.; Montag, D.; Groneberg, D. A.; Dhimal, M.; Kuch, U.; Müller, R. Spatial modelling of malaria cases associated with environmental factors in South Sumatra, Indonesia. *Malaria Journal* **2018**, 17 (1), 1–15.

(55) Cristofanelli, P.; Bonasoni, P.; Collins, W.; Feichter, J.; Forster, C.; James, P.; Kentarchos, A.; Kubik, P. W.; Land, C.; Meloen, J.; Roelofs, G. J.; Siegmund, P.; Sprenger, M.; Schnabel, C.; Stohl, A.; Tobler, L.; Tositti, L.; Trickl, T.; Zanis, P. Stratosphere-to-troposphere transport: A model and method evaluation. *Journal of Geophysical Research Atmospheres* **2003**, *108* (12).

(56) Wespes, C.; Hurtmans, D.; Emmons, L. K.; Safieddine, S.; Clerbaux, C.; Edwards, D. P.; Coheur, P.-F. Ozone variability in the troposphere and the stratosphere from the first 6 years of IASI observations (2008–2013). *Atmospheric Chemistry and Physics* **2016**, *16* (9), 5721–5743.

(57) Bastmeijer, K. Tourism in Antarctica: Increasing Diversity and the Legal Criteria for Authorisation. *New Zealand Journal of Environmental Law* **2003**, *7* (March 2007), 85–118.